A "CHANGING CHART" SYMPLECTIC ALGORITHM FOR RIGID BODIES AND OTHER HAMILTONIAN SYSTEMS ON MANIFOLDS

GIANCARLO BENETTIN*, ANNA MARIA CHERUBINI†, AND FRANCESCO FASSÒ‡

Abstract. We revive the elementary idea of constructing symplectic integrators for Hamiltonian flows on manifolds by covering the manifold with the charts of an atlas, implementing the algorithm in each chart (thus using coordinates), and switching among the charts whenever a coordinate singularity is approached. We show that this program can be implemented successfully by using a splitting algorithm, if the Hamiltonian is the sum $H_1 + H_2$ of two (or more) integrable Hamiltonians. Profiting of integrability, we compute exactly the flows of H_1 and H_2 in each chart and thus compute the splitting algorithm on the manifold by means of its representative in any chart. This produces a symplectic algorithm on the manifold which possesses an interpolating Hamiltonian, and hence has excellent properties of conservation of energy. We exemplify the method for a point constrained to the sphere and for a symmetric rigid body under the influence of positional potential forces.

Key words. Symplectic integrators, constrained Hamiltonian systems, rigid body.

AMS subject classifications. 65P10, 70H99, 70E17

1. Introduction and description of the method. Symplectic integrators are currently very popular for Hamiltonian systems, particularly in view of their stability and excellent energy conservation. Since the phase space of a number of Hamiltonian systems of relevant interest (e.g. rigid bodies) is not the Euclidean space $\mathbb{R}^{2n}$, but a symplectic manifold M, symplectic integrators on manifolds are of special importance.

If a manifold does not possess a single, global system of coordinates, integrations performed using coordinates must necessarily deal with the presence of coordinate singularities. Probably, the simplest idea for overcoming this situation is to consider a number of different systems of coordinates which have the singularities in different positions and hence form an atlas for M. One then implements an algorithm within each coordinate system and switches from one to the other, during the integration, whenever a coordinate singularity is approached. A "changing–chart" method of this kind has been indeed used in early molecular dynamics integrations of diatomic molecules [1] (in which case the manifold M is the cotangent bundle of the two–dimensional sphere), but the adopted algorithm was not symplectic. In fact, as noticed e.g. in [13], even using a symplectic algorithm in each chart, for instance a leap–frog, does not necessarily produce an algorithm on the manifold which has the stability and energy conservation of symplectic algorithms.[1]

To our knowledge, no symplectic "changing–chart" method has ever been developed. From the (vast) literature on the subject, one receives the impression that the presence of singularities has been generally felt as a serious difficulty for any approach based on the use of local coordinates (e.g., Euler angles in the rigid body case). A

---

*Università di Padova, Dipartimento di Matematica Pura e Applicata, GNFM, and INFM, Via G. Belzoni 7, 35131 Padova, Italy (`benettin@math.unipd.it`).

†Università di Lecce, Dipartimento di Matematica, and GNFM, Via per Arnesano, 73100 Lecce, Italy (`anna.cherubini@unile.it`).

‡Università di Padova, Dipartimento di Matematica Pura e Applicata, and GNFM, Via G. Belzoni 7, 35131 Padova, Italy (`fasso@math.unipd.it`). Partially supported by the EU contract HPRN-CT-2000-0113 for the project *MASIE – Mechanics and Symmetry in Europe.*

[1] More precisely, of symplectic integrators which possess a global interpolating Hamiltonian, see § 2.A below.

variety of alternative "geometric" approaches have thus been developed. A number of them share the common idea of embedding the manifold M in a higher dimensional space $\mathbb{R}^{2N}$ for some $N > n$, where $2n$ is the dimension of M (see e.g. [6] [7] [12] [13] [14] [15] [16] [17]); this achieves the goal of obtaining a global parametrization, but at the price of introducing more variables. In addition, the confinement to M has to be enforced in some way: for instance, the so called RATTLE algorithm, successfully applied in particular to the rigid body, resorts to the use of $2(N-n)$ Lagrange multipliers, so the number of variables to be managed further increases.[2] Moreover, these geometric algorithms are often implicit, i.e., numeric inversions are necessary at each time step. Nevertheless, in the literature these "geometric" schemes are generally considered superior to "changing–charts" methods.

In this article we propose a different point of view, namely we suggest that:

i. It is possible to implement "changing–chart" symplectic algorithms, by simply *choosing the algorithms in the individual charts in such a way that they are the local representatives of a symplectic map on the manifold.* This is indeed enough to assure, as is crucial, that the trajectories computed in the local charts are the local representatives of trajectories of a symplectic map on the manifold (the "geometric integrator"); all properties of the map are then automatically preserved, up to the round-off errors, by the local algorithms.

ii. A natural way of implementing this program is by means of the so called "splitting methods"; morever, such an implementation assures the existence on the manifold of the so called "interpolating Hamiltonian" — a rather crucial fact for symplectic integrators.

iii. In various situations, this leads to computationally efficient explicit algorithms, which are competitive with other "geometric" algorithms.

We will discuss theoretically the method in § 2. In addition, in § 3 we will illustrate the method by means of two examples, which are of interest, for instance, in molecular dynamics and in celestial mechanics. The first example is the point constrained to a sphere and subject to conservative forces, for which $M = T^*S^2$. The second is the symmetric rigid body in a positional conservative force field; assuming for the purpose of the discussion that the body has a fixed point, then $M = T^*\mathrm{SO}(3)$. We will use an atlas for the sphere made of two systems of spherical coordinates and an atlas for SO(3) made of two systems of Euler angles.

We now shortly describe the method. We use the following notations: if (M,σ) is a symplectic manifold and $F : M \to \mathbb{R}$ is a smooth function, then we denote by Φ_ϵ^F the map at time ϵ of the flow of the Hamiltonian vector field X_F of F; as is well known, for each ϵ, Φ_ϵ^F is a symplectic diffeomorphism from M to itself (the vector field X_F is assumed to be complete).

The splitting methods, see e.g. [18] [19] [17], are based on the idea of decomposing the Hamiltonian as the sum of two or more terms, the flows of which are easily computable. If

$$H = H_1 + H_2\,,$$

then the map

$$\Psi_\epsilon = \Phi_{\epsilon/2}^{H_2} \circ \Phi_\epsilon^{H_1} \circ \Phi_{\epsilon/2}^{H_2} \tag{1.1}$$

[2]For the rigid body, schemes using quaternions ([6], [7]) only require a normalization of the quaternion, but this seems to destroy symplecticity.

is easily seen to be a symplectic map from M to M, which differs from the flow Φ_ϵ^H of H by terms of order ϵ^3. So, Ψ_ϵ is a symplectic algorithm of second order on the manifold (higher order splitting methods can be constructed, see [18] [19]). In our application to the two problems mentioned above, we shall take as H_1 and H_2 the kinetic energy and, respectively, the potential energy. Both H_1 and H_2 are then individually integrable, and even more, exact explicit expressions of $\Phi_\epsilon^{H_1}$ and $\Phi_{\epsilon/2}^{H_2}$ in coordinates, actually very manageable ones, are easily written (H_1 corresponds in one case to the geodesic motion on the sphere, in the other case to the Euler–Poinsot motion of the free rigid body, while in both cases H_2 is independent of momenta and so trivially integrable). The fact that $\Phi_\epsilon^{H_1}$ and $\Phi_{\epsilon/2}^{H_2}$ are computed exactly (up to the round-off errors) in each coordinate system, automatically fulfills the above requirement (i). In other cases, like the triaxial rigid body, the kinetic energy H_1 is still integrable, but computing $\Phi_\epsilon^{H_1}$ requires handling elliptic functions. In such cases a further convenient splitting of H_1, leading to more manageable expressions, could be preferable; we shall come back on this point in the Conclusions.

As a final remark, we mention that the use of the splitting algorithm (1.1) to integrate the motion of a (tri–axial) rigid body has already been proposed in [17] [16] [15]; the first of these references also contains numerical integrations of rigid body motions. The two approaches, however, though similar for the use of (1.1), differ in the main point: namely we implement Ψ_ϵ in coordinates (two systems of Euler angles), while the point of view of the mentioned references is that, in order to avoid the coordinate singularities, one should implement the algorithm in a "geometric" way, specifically, using a Lie–Poisson integrator (coupled to the consideration of either rotational matrices or quaternions for the body orientation).

2. Theoretical description of the method. The good energy conservation of a class of symplectic algorithms is explained in terms of the existence of an "interpolating Hamiltonian flow". We begin by showing that this is the case for the splitting method on a manifold. In this context, it is important to distinguish between Hamiltonian and locally Hamiltonian flows (see the Remark below for some comments). Recall that a vector field X on a symplectic manifold (M,σ) is called *Hamiltonian* if the one–form $\sigma(X,\cdot)$ is exact, and *locally Hamiltonian* if this one–form is only closed. In the former case there exists a Hamiltonian function, namely a function $H: M\to\mathbb{R}$ such that $\sigma(X,\cdot)=-dH$; in the latter case, such functions exist only locally.

By a *one–parameter family of analytic symplectic diffeomorphisms* on an analytic symplectic manifold (M,σ) we mean an analytic map

$$\Psi: I\times M\to M\,, \qquad (\epsilon,m)\mapsto\Psi_\epsilon(m)\,,$$

where $I\subset\mathbb{R}$ is an interval containing zero, such that $\Psi_0=$ identity and, for any $\epsilon\in I$, Ψ_ϵ is an analytic symplectic diffeomorphism. An elementary generalization of known results for the Euclidean case $M=\mathbb{R}^{2n}$, $\sigma=\sum_i dp_i\wedge dq_i$, gives:

PROPOSITION 1. *Let Ψ_ϵ be a one–parameter family of analytic symplectic diffeomorphisms on a symplectic manifold (M,σ). Then, for any ϵ sufficiently near zero:*

i. *There exists a locally Hamiltonian ("interpolating") vector field X_ϵ such that*

$$\Psi_\epsilon=\Phi_\epsilon^{X_\epsilon}+\mathcal{O}\big(e^{-1/\epsilon}\big)\,. \tag{2.1}$$

Assume moreover that Ψ_ϵ is a composition of a finite number of flows of analytic Hamiltonian vector fields, each acting for a time which depends analytically on ϵ:

$$\Psi_\epsilon=\Phi_{\epsilon_1(\epsilon)}^{F_1}\circ\Phi_{\epsilon_2(\epsilon)}^{F_2}\circ\cdots\circ\Phi_{\epsilon_s(\epsilon)}^{F_s}$$

for analytic functions $\epsilon_j(\epsilon)$ which vanish at $\epsilon = 0$ and analytic functions $F_j : M \to \mathbb{R}$. Then:

ii. *The vector field X_ϵ is Hamiltonian.*

iii. *If Ψ_ϵ is an algorithm of order $r \geq 1$ for a given Hamiltonian H, that is*

$$\Psi_\epsilon = \Phi_\epsilon^H + \mathcal{O}(\epsilon^{r+1}),$$

then the Hamiltonian K_ϵ of X_ϵ satisfies

$$K_\epsilon = H + \mathcal{O}(\epsilon^r). \tag{2.2}$$

Proof. First note that all statements are true in the Euclidean case: statements (i) and (iii) are proven e.g. in [5], while statement (ii) is obvious since $\mathbb{R}^{2n}$ is simply connected. The fact that statements (i) and (iii) remain true on a manifold is seen by observing that, within the quoted proof, X_ϵ and K_ϵ are constructed as formal series the coefficients of which are commutators of vector fields and Poisson brackets of functions, respectively. Since these objects are intrinsically defined on the manifold (i.e., their local representatives commute with the change of charts), the argument of [5] applies as is to the case of a manifold. Estimates, which allow one going beyond the formal level and obtaining (2.1), are performed locally, within each chart (analyticity is required for this).

Let us now prove statement (ii). Consider for simplicity the case of the composition of two flows. Then, formally

$$\Phi_{\epsilon_1}^{X_1} \circ \Phi_{\epsilon_2}^{X_2} = \Phi_1^{\epsilon_1 X_1} \circ \Phi_1^{\epsilon_2 X_2} = \Phi_1^X$$

for a vector field X which is given, as a formal series, by the BCH formula. The fact that, if X_1 and X_2 are Hamiltonian then X is also Hamiltonian, not only locally Hamiltonian, is seen by observing that the terms of the BCH series are built up of commutators of X_1 and X_2 and recalling that the commutator of two Hamiltonian vector fields is Hamiltonian (the Hamiltonian is the Poisson bracket of the Hamiltonians of X_1 and X_2). The extension to any number of flows is obvious. $\square$

The Hamiltonian K_ϵ is called the *interpolating Hamiltonian* of the algorithm Ψ_ϵ (*modified Hamiltonian* is also used). The existence of the interpolating Hamiltonian explains the very good energy conservation of symplectic algorithms. Up to quantities $\mathcal{O}(e^{-1/\epsilon})$, which can be easily made smaller than the round–off even in multiple precision [2] by taking the step–size ϵ small enough, the iteration of the symplectic integrator follows exactly the flow of the nearby vector field X_ϵ. If this vector field is Hamiltonian (not just locally Hamiltonian), then its Hamiltonian K_ϵ is preserved by the algorithm, up to an exponentially small error. Accumulation of these extremely small errors produces acceptable overall effects on significantly long integration times.[3]

Remark: The distinction between the existence of a Hamiltonian interpolating vector field and a locally Hamiltonian one is important, even though so far it has not drawn much attention (for some results see [5] and [8]). A locally Hamiltonian interpolating vector field does not assure energy conservation: any local interpolating Hamiltonian is conserved by the algorithm, but this conservation law might be broken by orbits winding around the manifold. Of course, the problem does not exist in

[3] In *special* situations, the errors on the energy do not accumulate: see [5] and, for numerical results, [2].

$$
\begin{tikzcd}
& M \arrow[dl, "z"'] \arrow[dr, "z'"] & \\
\mathbb{R}^{2n} \arrow[rr, "\mathcal{C}"] \arrow[d, "\psi_\epsilon"] & & \mathbb{R}^{2n} \arrow[d, "\psi'_\epsilon"] \\
\mathbb{R}^{2n} \arrow[rr, "\mathcal{C}"] & & \mathbb{R}^{2n}
\end{tikzcd}
$$

FIG. 1. *The local representatives of the algorithm commute with the change of charts.*

the Euclidean case, because of the simply connectedness of $\mathbb{R}^{2n}$. However, simple examples demonstrate that, on a manifold, some condition is necessary to assure the Hamiltonian character of the interpolating vector field (e.g., $M = \mathbb{R} \times S^1 \ni (I, \varphi)$, $\sigma = dI \wedge d\varphi$, $\Psi_\epsilon(I, \varphi) = (I + \epsilon, \varphi)$).

By Proposition 1, the algorithm Ψ_ϵ on M defined by (1.1) has a global interpolating Hamiltonian $K_\epsilon = H_1 + H_2 + \mathcal{O}(\epsilon^2)$. This fact alone makes clear that, however implemented in local coordinates, this algorithm will exhibit good energy conservation.

For the sake of the discussion, assume that M has a symplectic atlas which consists of just two charts, with coordinates $z = (q, p)$ and $z' = (q', p')$. Let $\mathcal{C}$ be the change of chart, so that $z' = \mathcal{C} \circ z$. If $h = h_1 + h_2$ and $h' = h'_1 + h'_2$ are the local representatives of the Hamiltonian $H = H_1 + H_2$ in the two charts,[4] then the local representatives ψ_ϵ and ψ'_ϵ of the map Ψ_ϵ are

$$\psi_\epsilon = \Phi^{h_2}_{\epsilon/2} \circ \Phi^{h_1}_{\epsilon} \circ \Phi^{h_2}_{\epsilon/2}\,, \qquad \psi'_\epsilon = \Phi^{h'_2}_{\epsilon/2} \circ \Phi^{h'_1}_{\epsilon} \circ \Phi^{h'_2}_{\epsilon/2}\,.$$

By construction, these two maps commute with the change of chart, i.e.

$$\mathcal{C} \circ \psi_\epsilon = \psi'_\epsilon \circ \mathcal{C} \tag{2.3}$$

(see figure 1). It follows that *we can freely switch from one chart to the other, and keep following the iteration of the map Ψ_ϵ on the manifold.* In other words, this "changing–chart" method is an actual implementation of the algorithm (1.1) on the manifold. Note that the coordinate systems used, and the adopted criterion for when to switch chart, are completely immaterial: different choices may produce more or less simple and efficient implementations, but do not affect the algorithm.[5] The implementations

[4]This means that the restriction of H to the first chart equals $h \circ z$, etc. Note that $h = h' \circ \mathcal{C}$ in the intersection of the chart domains.

[5]In fact, it is not even necessary that the coordinates z and z' be symplectic, even though this is likely to be the simplest choice. If the coordinates are not symplectic, one should repeat the previous argument by considering not the Hamiltonians and their local representatives, but the corresponding Hamiltonian vector fields.

of the changing chart methods mentioned in the Introduction did not satisfy (2.3), and this makes the difference.

In the next section we illustrate this procedure on the two cases mentioned in the Introduction, in which H_1 is the kinetic energy of an integrable system and H_2 is a positional potential. The flow of H_2 is trivially integrated: if $h_2(q)$ is the local representative of H_2 in a chart with coordinates (p,q), then

$$(p,q) \mapsto \Big(p + t\,\frac{\partial h_2}{\partial q}(q), q\Big)\,.$$

The local representatives of H_1 depend on both coordinates and momenta, but since H_1 is integrable, in principle one knows the solution in each chart. The crucial step, on which the efficiency of the algorithm relies, is to have an analytical representation of the flow $\Phi_\epsilon^{H_1}$ of the kinetic energy which is suitable for numerical computations.

3. Two Examples.

3.1. The point constrained to the sphere. As a first elementary example, we consider a point constrained to the unit sphere in $\mathbb{R}^3$, subject to positional potential forces. The flow $\Phi_\epsilon^{H_1}$ of the kinetic energy is the geodesic flow on the sphere and is easily written in any system of coordinates. We used two systems of spherical coordinates and the corresponding momenta, that we denote $(\varphi,\theta,p_\varphi,p_\theta)$ and $(\varphi',\theta',p'_\varphi,p'_\theta)$, relative to two orthogonal frames $\{e_x,e_y,e_z\}$ and, respectively, $\{e'_x,e'_y,e'_z\} = \{e_x,-e_z,e_y\}$. The change of charts are given by

$$\begin{cases} \cos\theta = -\sin\theta'\,\sin\varphi' \\ \sin\theta = \sqrt{1-\cos^2\theta} \\ \cos\varphi = \frac{\sin\theta'\,\cos\varphi'}{\sin\theta} \\ \sin\varphi = \frac{\cos\theta'}{\sin\theta} \\ p_\theta = \frac{\cos\theta'\,\sin\varphi'}{\sin\theta}\,p'_\theta + \frac{\cos\varphi'}{\sin\theta\,\sin\theta'}\,p'_\varphi \\ p_\varphi = -\cos\varphi'\,p'_\theta + \frac{\sin\varphi'\,\cos\theta'}{\sin\theta'}\,p'_\varphi \end{cases}\,, \qquad \begin{cases} \cos\theta' = \sin\theta\,\sin\varphi \\ \sin\theta' = \sqrt{1-\cos^2\theta'} \\ \cos\varphi' = \frac{\sin\theta\,\cos\varphi}{\sin\theta'} \\ \sin\varphi' = -\frac{\cos\theta}{\sin\theta'} \\ p'_\theta = -\frac{\cos\theta\,\sin\varphi}{\sin\theta'}\,p_\theta - \frac{\cos\varphi}{\sin\theta\,\sin\theta'}\,p_\varphi \\ p'_\varphi = \cos\varphi\,p_\theta - \frac{\sin\varphi\,\cos\theta}{\sin\theta}\,p_\varphi \end{cases}\,.$$

Due to rotational invariance, both the kinetic energy and the geodesic flow have the same expression in the two charts, so we write them down only in the first chart. The kinetic energy is

$$h_1(\varphi,\theta,p_\varphi,p_\theta) = \frac{p_\theta^2}{2} + \frac{p_\varphi^2}{2\sin^2\theta}\,.$$

The geodesic flow is determined either by integrating Hamilton's equations, or just by observing that it consists of a uniform translation along a great circle. Consider the initial datum $(\varphi(0),\theta(0),p_\varphi(0),p_\theta(0)) = (\varphi_0,\theta_0,J,P_0)$, and denote

$$G = \sqrt{P_0^2 + \Big(\frac{J}{\sin\theta_0}\Big)^2}\,, \qquad \hat P_0 = \frac{P_0}{G}\,, \qquad \hat J = \frac{J}{G}\,;$$

G is the norm of the angular momentum and, as p_φ, is an integral of motion (this is the reason why we do not append the subscript 0 to G and J). Then, the solution $(\varphi(t),\theta(t),p_\varphi(t),p_\theta(t))$ of the system with Hamiltonian h_1 can be written as

$$\begin{pmatrix} \cos\theta(t) \\ \frac{p_\theta(t)}{G}\sin\theta(t) \end{pmatrix} = \begin{pmatrix} \cos Gt & -\sin Gt \\ \sin Gt & \cos Gt \end{pmatrix} \begin{pmatrix} \cos\theta_0 \\ \hat P_0 \sin\theta_0 \end{pmatrix}$$

$$\begin{pmatrix} \cos\varphi(t) \\ \sin\varphi(t) \end{pmatrix} = \frac{1}{\sin\theta(t)} \begin{pmatrix} C & -S \\ S & C \end{pmatrix} \begin{pmatrix} \cos\varphi_0 \\ \sin\varphi_0 \end{pmatrix}$$

for

$$C = \sin\theta_0 \, \cos Gt + \hat{P}_0 \, \cos\theta_0 \, \sin Gt$$
$$S = \frac{\hat{J}}{\sin\theta_0} \, \sin Gt$$

3.2. The symmetric rigid body. We consider now the symmetric rigid body with a fixed point (symmetric just means here that two of the three moments of inertia relative to the fixed point are equal). Let $\{e_1, e_2, e_3\}$ be an orthogonal frame centered on the body's fixed point with axes oriented like the principal axes of inertia, and let $I_1 = I_2$ and I_3 be the corresponding principal moments of inertia. In order to obtain an atlas for $T^*\mathrm{SO}(3)$ we consider two systems of standard Euler angles (see figure 2), say $q = (\varphi, \psi, \theta)$ and $q' = (\varphi', \psi', \theta')$, relative to different spatial frames $\{e_x, e_y, e_z\}$ and respectively $\{e'_x, e'_y, e'_z\} = \{e_z, e_x, e_y\}$. These coordinates and their conjugate momenta $p = (p_\varphi, p_\psi, p_\theta)$ and $p' = (p'_\varphi, p'_\psi, p'_\theta)$ are related by the equations

$$\begin{cases} \cos\theta = \sin\theta' \, \sin\varphi' \\ \sin\theta = \sqrt{1-\cos^2\theta} \\ \cos\varphi = -\cos\theta' / \sin\theta \\ \sin\varphi = -\sin\theta' \, \cos\varphi' / \sin\theta \\ \cos\psi = -(\cos\varphi' \, \sin\psi' \\ \qquad\quad + \cos\theta' \, \sin\varphi' \, \cos\psi') / \sin\theta \\ \sin\psi = (\cos\varphi' \, \cos\psi' \\ \qquad\quad - \cos\theta' \, \sin\varphi' \, \sin\psi') / \sin\theta \\ p_\theta = -\frac{\sin\varphi' \cos\theta'}{\sin\theta} p'_\theta \\ \qquad\quad - \frac{\cos\varphi'}{\sin\theta \sin\theta'} (p'_\varphi + \cos\theta' p'_\psi) \\ p_\varphi = \cos\varphi \, p'_\theta - \frac{\sin\varphi'}{\sin\theta'} (\cos\theta' p'_\varphi + p'_\psi) \\ p_\psi = p'_\psi \end{cases} \qquad \begin{cases} \cos\theta' = -\sin\theta \, \cos\varphi \\ \sin\theta' = \sqrt{1-\cos^2\theta'} \\ \cos\varphi' = -\sin\theta \sin\varphi / \sin\theta' \\ \sin\varphi' = \cos\theta / \sin\theta' \\ \cos\psi' = -(\sin\varphi \, \sin\psi \\ \qquad\quad - \cos\theta \, \cos\varphi \, \cos\psi) / \sin\theta' \\ \sin\psi' = (\sin\varphi \, \cos\psi \\ \qquad\quad + \cos\theta \, \cos\varphi \, \sin\psi) / \sin\theta' \\ p'_\theta = \frac{\cos\varphi \cos\theta}{\sin\theta'} p_\theta \\ \qquad\quad - \frac{\sin\varphi}{\sin\theta \sin\theta'} (p_\varphi - \cos\theta \, p_\psi) \\ p'_\varphi = \sin\varphi \, p_\theta \\ \qquad\quad + \frac{\cos\varphi}{\sin\theta} (\cos\theta p_\varphi + p_\psi) \\ p'_\psi = p_\psi \end{cases}$$

Here too the kinetic energy has the same form in both coordinate systems, precisely

$$h_1(q,p) = \frac{p_\theta^2}{2I_1} + \frac{(p_\varphi - p_\psi \cos\theta)^2}{2I_1 \sin^2\theta} + \frac{p_\psi^2}{2I_3} \, .$$

The components of the angular momentum along the axes e_z and e_3, namely p_φ and p_ψ, are constants of motion of the free system; their values will be hereafter denoted J and L, respectively. Also the norm G of the angular momentum vector is constant; one has

$$G = \sqrt{p_\theta^2 + p_\psi^2 + \Big(\frac{p_\varphi - p_\psi \cos\theta}{\sin\theta}\Big)^2} \, . \tag{3.1}$$

In the classical textbooks and manuals we consulted, we found the expression of the solution of the Euler–Poinsot system only in special systems of Euler angles, with the spatial axis e_z parallel to the angular momentum. Since this is not sufficient for our purposes, we computed the solution in a generic system of Euler angles (this is elementary in the symmetric case):

PROPOSITION 2. *Consider an initial datum* $(\varphi(0), \psi(0), \theta(0), p_\varphi(0), p_\psi(0), p_\theta(0)) = (\varphi_0, \psi_0, \theta_0, J, L, P_0)$*, and let* G *be the corresponding norm of the angular momentum.*

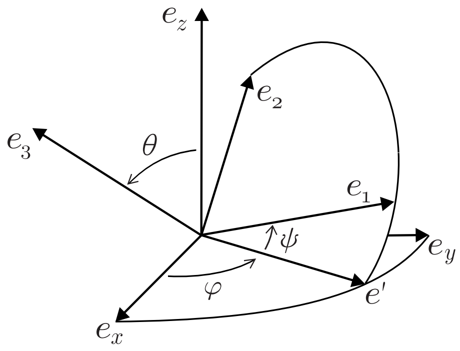

FIG. 2. *The Euler angles φ, ψ, θ (e' is the unit vector in the direction of $e_z \times e_3$).*

Denote

$$\hat{J} = \frac{J}{G}, \qquad \hat{L} = \frac{L}{G}, \qquad \hat{P}_0 = \frac{\hat{P}_0}{G}, \qquad \Omega = \frac{G}{I_1}, \qquad \Lambda = \frac{I_1 - I_3}{I_1 I_3} L .$$

Then, for all t such that $\sin\theta(t) \neq 0$, the solution of the system of Hamiltonian h_1 is given by

$$\begin{pmatrix} \cos\theta(t) - \hat{J}\hat{L} \\ \frac{p_\theta(t)}{G}\sin\theta(t) \end{pmatrix} = \begin{pmatrix} \cos\Omega t & -\sin\Omega t \\ \sin\Omega t & \cos\Omega t \end{pmatrix} \begin{pmatrix} \cos\theta_0 - \hat{J}\hat{L} \\ \hat{P}_0 \sin\theta_0 \end{pmatrix} \tag{3.2}$$

$$\begin{pmatrix} \cos\varphi(t) \\ \sin\varphi(t) \end{pmatrix} = \frac{1}{\sin\theta_0 \, \sin\theta} \begin{pmatrix} C(\hat{J},\hat{L}) & S(\hat{J},\hat{L}) \\ -S(\hat{J},\hat{L}) & C(\hat{J},\hat{L}) \end{pmatrix} \begin{pmatrix} \cos\varphi_0 \\ \sin\varphi_0 \end{pmatrix} \tag{3.3}$$

$$\begin{aligned} \begin{pmatrix} \cos\psi(t) \\ \sin\psi(t) \end{pmatrix} = \frac{1}{\sin\theta_0 \, \sin\theta} & \begin{pmatrix} C(\hat{L},\hat{J}) & S(\hat{L},\hat{J}) \\ -S(\hat{L},\hat{J}) & C(\hat{L},\hat{J}) \end{pmatrix} \\ & \times \begin{pmatrix} \cos\Lambda t & -\sin\Lambda t \\ \sin\Lambda t & \cos\Lambda t \end{pmatrix} \begin{pmatrix} \cos\psi_0 \\ \sin\psi_0 \end{pmatrix} \end{aligned} \tag{3.4}$$

where

$$\begin{aligned} C(x,y) = {} & y(y - x\cos\theta_0) \\ & + \left[\sin^2\theta_0 - y(y - x\cos\theta_0)\right]\cos\Omega t + \hat{P}_0 \sin\theta_0 \cos\theta_0 \sin\Omega t \end{aligned} \tag{3.5}$$

$$S(x,y) = (1 - \cos\Omega t)\hat{P}_0 \sin\theta_0 y + (x - y\cos\theta_0)\sin\Omega t . \tag{3.6}$$

A proof of this Proposition is given in the Appendix.

Remark: If the algorithm is regarded as mapping sine and cosine of the angles at time zero to sine and cosine of the angles at time t, then only four trigonometric functions must be computed, namely sine and cosine of Ωt and of Λt; all other operations are algebraic (elementary operations, and a few square roots). Developing an efficient, accurate algorithm for the symmetric rigid body was the original motivation of this work. We were interested in performing long–time integrations of rigid bodies under generic potential force fields, so as to investigate the presence of the chaotic behaviour predicted in the works [3] and [4]. We will publish the results of these integrations somewhere else. We just mention here that the algorithm appeared to be simple, efficient, stable. Overall, it seemed to perform exceptionally well.

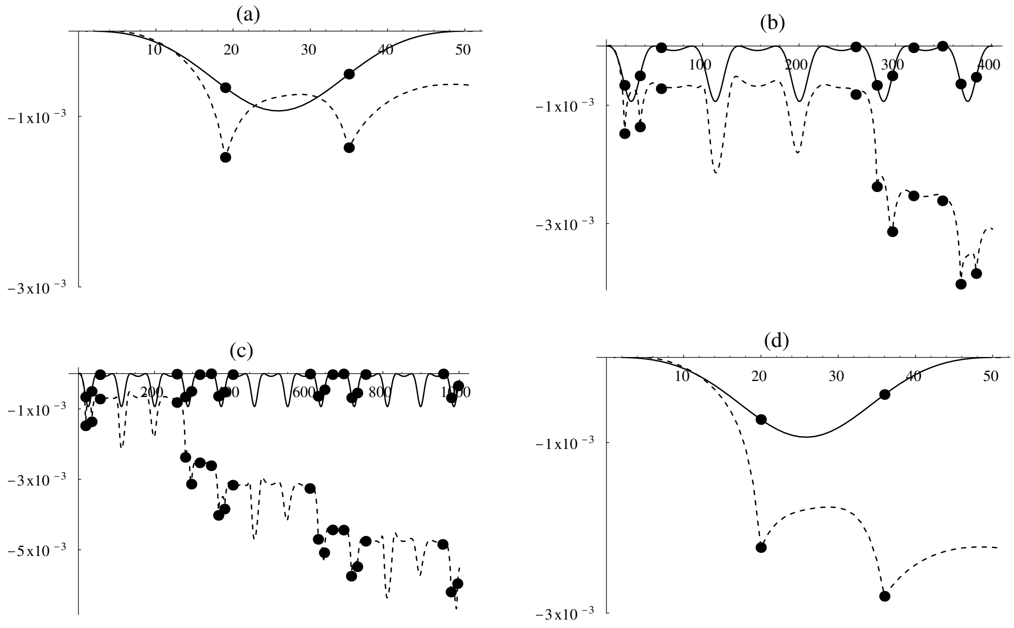

FIG. 3. *Error in the energy along an orbit of the spherical pendulum for our algorithm (solid line) and for a pair of leapfrog (dotted line). Charts are switched when* $\arcsin\theta$ *reaches* 0.7 *in (a), (b) and (c), and* 0.5 *in (d).*

4. Numerical tests and comparisons. Our algorithm exhibits the typical very good conservation of energy of the symplectic algorithms which possess an interpolating Hamiltonian.

The best way of illustrating this fact and of enlightening the mechanism underneath, is probably by means of the comparison with a slightly (but crucially) different algorithm. Specifically, we consider within each chart a (generalized) leapfrog, namely the map $\tilde\psi^h_\epsilon = \tilde\psi^h_{II} \circ \tilde\psi^h_I$ where $\tilde\psi^h_I : (q,p) \mapsto (q^I, p^I)$ and $\tilde\psi^h_{II} : (q^I,p^I) \mapsto (q^{II},p^{II})$ are (implicitly) defined by

$$\tilde\psi^h_I : \begin{cases} p^I = p - \frac{\epsilon}{2}\frac{\partial h}{\partial q}(p^I,q) \\ q^I = q + \frac{\epsilon}{2}\frac{\partial h}{\partial p}(p^I,q) \end{cases}, \qquad \tilde\psi^h_{II} : \begin{cases} q^{II} = q^I + \frac{\epsilon}{2}\frac{\partial h}{\partial p}(p^I,q^{II}) \\ p^{II} = p^I - \frac{\epsilon}{2}\frac{\partial h}{\partial q}(p^I,q^{II}) \end{cases}. \tag{4.1}$$

The standard leap-frog (or Verlet) algorithm is obtained when $h(q,p)$ is separated, namely $h(q,p) = h_1(p) + h_2(q)$; in such a case, as we have already mentioned, this algorithm also coincides with the splitting algorithm (1.1). In the two cases considered above, the point on the sphere in polar coordinates and the symmetric rigid body in Euler angles, the Hamiltonians are not separated but the generalized leapfrogs $\tilde\psi^h_\epsilon$ and $\tilde\psi^{h'}_\epsilon$ in the two charts are anyway explicit.

As is well known, the generalized leapfrog $\tilde\psi^h_\epsilon$ in each chart is symplectic, possesses an interpolating Hamiltonian, and differs from Φ^h_ϵ by $\mathcal{O}(\epsilon^3)$. *However, the two generalized leapfrogs do not commute with the change of chart, namely,* $\mathcal{C}\circ\tilde\psi^h_\epsilon \neq \tilde\psi^{h'}_\epsilon \circ \mathcal{C}$. This means that the two algorithms are not the local representatives of a single algorithm on the manifold. In particular, *the interpolating Hamiltonians of the individual*

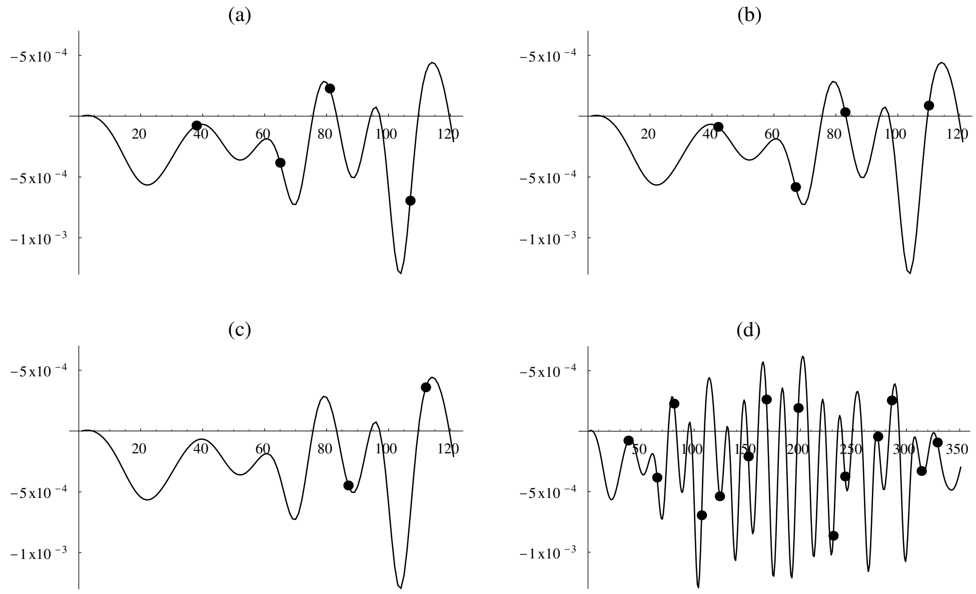

FIG. 4. *Error in the energy along an orbit of the symmetric rigid body in an external potential, computed with our algorithm. The chart is switched when* $\arcsin\theta$ *reaches* 0.7 *in (a) and (d),* 0.5 *in (b), and* 0.2 *in (c).*

algorithms in the two charts are not the local representatives of a single function on the manifold. The consequence is that each change of chart introduces a change of order ϵ^2 in the conserved quantity (i.e., the interpolating Hamiltonian of the local algorithm) and this results typically in a progressive drift of the energy, proportional to ϵ^2 and to the number of chart changes.[6]

This is illustrated in figure 3, which refers to the simple case of the spherical pendulum, namely a heavy point on the sphere; the potential energy in the two charts are $h_2 = \cos\theta$ and $h_2' = -\sin\theta' \sin\varphi'$. All figures report the relative error in the energy along the same orbit, which has been computed with the splitting algorithm (solid line) and switching between the two generalized leapfrogs (dotted line). The two methods are implemented using the same coordinate systems, the same criterion for switching chart, and the same integration step. The superimposed dots identify the instants at which the chart is switched. In all figures the initial datum is $(\varphi, \theta, p_\varphi, p_\theta) = (\pi/3, \pi/3, 1.1, 0.35)$ (in the first chart) and the integration step is $\epsilon = 0.05$. Figures 3.a, 3.b and 3.c differ only for the total integration time, which equals 50, 400 and 1000 time steps, respectively. The difference between the two methods is evident: switching charts has no consequence for the splitting algorithm, while it produces accumulation of errors for the pair of generalized leapfrogs.

In figures 3.a, 3.b and 3.c the chart was changed whenever the colatitude θ (or θ') reached the value arcsin(0.7). In figure 3.d we used a different criterion for changing chart, so as to force the change of charts at different instants. Specifically, we changed chart when the colatitude reached arcsin(0.5). Comparison with figure 3.a indicates

[6] This mechanism was already observed in [13].

that this has a consequence for the pair of generalized leapfrogs, but not for our algorithm, which is completely transparent to the change of chart.

The same behaviour is found in the symmetric rigid body. Figure 4 refers to a rigid body with moments of inertia $I_1 = I_2 = 1$ and $I_3 = 2/3$. The potential energy in the two Euler angles charts introduced in the previous section is

$$\begin{aligned} h_2(q,p) &= \sin\theta\cos\varphi + (\sin\theta\cos\psi)^2 \\ h_2'(q',p') &= -\sin\theta'\sin\varphi' + (\sin\varphi\sin\psi - \cos\varphi\cos\psi\cos\theta)^2 \,. \end{aligned}$$

Figures 4.a–4.c show the energy error on 120 time steps for the orbit with initial datum $(\varphi,\psi,\theta,p_\varphi,p_\psi,p_\theta) = (0.5,-0.45,\pi/3,2.2,0.8,1.3)$; the integration step is 0.05 in all cases, while the chart is switched when $\sin\varphi$ reaches the values 0.7, 0.5, 0.2, respectively. Figure 4.d is the same as figure 4.a, but for a longer integration time.

Remark: Figure 3 indicates that, even within a given chart, the error on the energy is smaller for the splitting algorithm than for the generalized leapfrog. This is largely due to the fact that, within our algorithm, the flow of the kinetic energy is computed exactly, what produces a more stable algorithm. In fact, the leapfrog has a factor $(\sin\theta)^{-3}$ which degrades the precision already at moderate distances from the singularities. The same situation is met with the symmetric rigid body: figures 4.a–4.c indicate that the energy conservation does not get worse when the singularities are approached (up to arcsin(0.2) in the case of figure 4.c). In this case too, the energy error with a pair of leapfrog is much bigger.

As a further evidence that the algorithm, though written in coordinates, is nevertheless coordinate independent, let us propose another elementary test. Consider a Lagrange top, that is a heavy symmetric rigid body, and let e_g be the unit vector in the direction of gravity. The component of the angular momentum along e_g, that we shall denote m, is then a constant of motion. Quite clearly, if we use a chart of Euler angles, relative to a spatial frame $\{e_x, e_y, e_z\}$ with $e_g = e_z$, then $m = p_\varphi$, and since the Hamiltonian is independent of φ, m is exactly conserved. Now, *since the algorithm commutes with the change of chart, the same must be true,* up to the round-off errors, *in any other chart,* for example a chart of Euler angles relative to a spatial frame $\{e_x, e_y, e_z\}$ such that e_g has no special direction. This is precisely what we found numerically: working in double precision, for several choices of e_g and of the initial data, the error we found in m, after many thousands of time-steps and hundreds of chart changes, was at most of order 10^{-13}, independently of the step–size, and reduced to 10^{-30} in quadruple precision. Such a specially good conservation law is not obvious, for a second order algorithm, and reflects in an essential way its geometrical nature, while the implementation in coordinates is irrelevant.

5. Conclusions. In our opinion, the method described here has potentially many advantages and is worth of further consideration.

A crucial fact, which is missing in the present analysis, is a comparison with other methods. We made some comparisons with RATTLE in the case of the point on the sphere, and found that the two algorithms perform in a comparable way. For the same step–size RATTLE was somewhat faster (by about a factor 1.5 to 2, depending on the potential), but our algorithm was more stable (the same energy conservation was obtained, typically, with a step–size bigger by a factor 1.5).

As is clear, this comparison is not conclusive. In the case of the rigid body, a thorough comparison with other methods (RATTLE [14] [12], Lie–Poisson integrators [17] [15] [16], and the methods of [10] [11]) is necessary and is in our programs.

As already remarked, in the case of the rigid body RATTLE is not explicit and the codimension $2(N-n)$ is 12; hence, the algorithm must handle 18 variables and in addition a total of 12 Lagrange multipliers.[7] Our algorithm instead uses only 6 variables, and for a symmetric rigid body it is explicit and fully manageable, requiring only the evaluation of four trigonometric functions at each time step. We expect in this case our algorithm to be faster (we guess significantly faster).

The situation is more delicate for the tri–axial rigid body. Since the representation of the Euler–Poinsot flow in Euler angles uses elliptic functions, the exact integration of the flow of the kinetic energy might significantly lengthen the integration time. Alternatives are based on the further splitting of the Euler–Poinsot Hamiltonian as the sum of two or more integrable Hamiltonians, each of which is (more) easily integrated. This approach was already proposed and used in [17] [15] [16], though, as already remarked, not using coordinates. Convenient splittings of the Euler–Poinsot system are expected to produce quite manageable algorithms, with good (perhaps slightly worse) stability. A careful analysis in our opinion is necessary to evaluate the different possibilities.

We prefer to leave these tests and comparisons to a dedicated work. In addition to such tests, of course, it is also important to experiment the performance of the algorithm in concrete problems, especially when accuracy is important. As we have already remarked in § 3, we are presently working on the symmetric rigid body, in order to evaluate the degree of optimality of some previous perturbative studies; such an investigation is numerically delicate, but the preliminary results are rather satisfying. Other studies, for example in molecular dynamics, would be of great interest.

In this regard, we should mention a further positive feature of the splitting method. The estimate (2.2) on the interpolating Hamiltonian given in Proposition 1 can be further detailed: $H-K_\epsilon$ is in fact of the order of ϵ^r times the biggest of (some norm of) the Poisson brackets $\{F_i,F_j\}$, $i,j=1,\ldots,s$. Consider now the case in which one has a nearly integrable Hamiltonian H, say

$$H = H_1 + \mu H_2 \,, \qquad \mu \ll 1 \,.$$

If one can integrate exactly the flow of H_1, then it is possible to use the second order splitting algorithm $\Phi^{H_2}_{\epsilon/2}\circ\Phi^{H_1}_{\epsilon}\circ\Phi^{H_2}_{\epsilon/2}$. In this case, the interpolating Hamiltonian gets the form

$$K_\epsilon = H_1 + \mu\big[H_2 + \mathcal{O}(\epsilon^2)\big] \,,$$

i.e., the correction due to the algorithm remains small with respect to the perturbation (as is obviously necessary in a perturbation problem) for small ϵ, with no need to reduce ϵ dependently on μ. This fact is especially useful if one is interested in exploring numerically the case $\mu\to 0$. Unfortunately, in the case of a triaxial body, this positive feature is destroyed by a splitting of the Euler–Poinsot Hamiltonian, so for very small μ the exact integration of H_1 via elliptic functions could become competitive.

Anyhow, beyond these special applications, it seems to us that the possibility described here of constructing "changing–chart" symplectic algorithms on manifolds, just by implementing splitting algorithms in coordinates, has a character of simplicity

[7] There are formulations of RATTLE which use fewer coordinates (e.g. the four Euler parameters, see [9]), so that these numbers can be drastically reduced, but to our knowledge they are not symplectic.

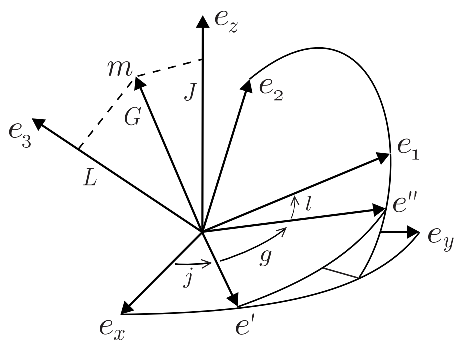

FIG. 5. *The action–angle coordinates of the symmetric Euler–Poinsot system; m is the angular momentum and e' and e'' are unit vectors in the directions of $e_z \times m$ and, respectively, of $m \times e_3$.*

which makes it of interest by itself, even independently of its performance in specific situations.

Appendix. Proof of Proposition 2. Probably, the simplest way of obtaining the expressions for the flow of the symmetric Euler–Poinsot system given in Proposition 2 is by referring to the "action–angle" coordinates (G, L, J, g, l, j) of the system, in which the flow is trivial. These coordinates, which are also known as Andoyer or Deprit coordinates, are defined as follows: G, L and J are respectively the length, the component along the symmetry axis and the component along the z–axis of the angular momentum vector; their three conjugate angles g, l and j are defined as shown in figure 5, where e_1, e_2, e_3 is an orthonormal frame fixed in the body, with e_3 along the symmetry axis. Clearly, these coordinates are singular when the angular momentum is aligned with either e_3 or e_z, namely for either $G = \pm L$ or $G = \pm J$.

The advantage of the action–angle coordinates is that the flow of the symmetric Euler–Poinsot system is linear in these coordinates. In fact, the Hamiltonian is

$$H(G, L) = \frac{1}{2I_1}\, G^2 + \frac{I_1 - I_3}{2I_1 I_3}\, L^2$$

and hence the flow is given by G, L, J, j constant and

$$g(t) = g_0 + \Omega\, t\,, \qquad l(t) = l_0 + \Lambda\, t \tag{A.1}$$

where $\Omega = G/I_1$ and $\Lambda = \frac{I_1 - I_3}{2I_1 I_3} L$. Obviously, this solution is valid as long as the system stays away from the singularities of the action–angle coordinates; this limitation will be eliminated below.

In order to prove the Proposition, we convert the flow written in action–angle coordinates to Euler angles. The formulas relating the Euler angles to the action–angle coordinates which are needed here are as follows:

$$G = \sqrt{p_\theta^2 + p_\psi^2 + \Big(\frac{p_\varphi - p_\psi \cos\theta}{\sin\theta}\Big)^2}\,, \qquad L = p_\psi\,, \qquad J = p_\varphi \tag{A.2}$$

$$\cos g = \frac{\hat{J}\,\hat{L} - \cos\theta}{\sqrt{1 - \hat{J}^2}\sqrt{1 - \hat{L}^2}}\,, \qquad \sin g = -\,\frac{p_\theta \sin\theta}{G\,\sqrt{1 - \hat{J}^2}\sqrt{1 - \hat{L}^2}} \tag{A.3}$$

$$j = \varphi + \alpha\,, \qquad l = \psi + \beta \tag{A.4}$$

where $\hat{J} = J/G$, $\hat{L} = L/G$, the angle α satisfies

$$\cos\alpha = \frac{\hat{L} - \hat{J}\cos\theta}{\sin\theta\sqrt{1-\hat{J}^2}}\,, \qquad \sin\alpha = \frac{p_\theta\,\sin\theta}{G\sqrt{G^2-J^2}}\,,$$

and the angle β satisfies these same expressions with $\hat{J}$ and $\hat{L}$ interchanged. These equalities are easily proven (see e.g. [3], where a few of them are proven). In the sequel, we use the notation

$$R_\delta = \begin{pmatrix} \cos\delta & -\sin\delta \\ \sin\delta & \cos\delta \end{pmatrix}\,.$$

Equations (A.3) and (A.1) together imply

$$\begin{pmatrix} \hat{J}\hat{L} - \cos\theta(t) \\ \frac{p_\theta(t)}{G}\sin\theta(t) \end{pmatrix} = R_{\Omega t}\begin{pmatrix} \hat{J}\hat{L} - \cos\theta(t) \\ \frac{p_\theta(0)}{G}\sin\theta(0) \end{pmatrix}$$

namely (3.2). Next, since $j = \varphi + \alpha$ one has

$$\begin{pmatrix} \cos\varphi(t) \\ \sin\varphi(t) \end{pmatrix} = R_{\alpha(t)}\begin{pmatrix} \cos j_0 \\ \sin j_0 \end{pmatrix} = R_{\alpha(t)}\,R_{-\alpha(0)}\begin{pmatrix} \cos\varphi_0 \\ \sin\varphi_0 \end{pmatrix}\,;$$

a trivial although somewhat lengthy computation shows that the product of the two matrices can be written in the form given in equation (3.3). Finally,

$$\begin{pmatrix} \cos\psi(t) \\ \sin\psi(t) \end{pmatrix} = R_{\beta(t)}\begin{pmatrix} \cos l(t) \\ \sin l(t) \end{pmatrix} = R_{\beta(t)}\,R_{-\beta(0)}\,R_{\Lambda t}\begin{pmatrix} \cos\psi_0 \\ \sin\psi_0 \end{pmatrix}$$

where we have used the fact that planar rotations commute; equation (3.4) is now obtained by observing that $R_{\beta(t)}R_{-\beta(0)}$ equals $R_{\alpha(t)}R_{-\alpha(0)}$ after switching $\hat{J}$ and $\hat{L}$.

In this way, we have proven the expressions (3.3)–(3.4) for times t such that the solution remains within the domain of the action–angle coordinates for all times $0 < t' < t$. But analyticity in t of the solution ensures that these expressions are in fact valid for all t such that $\sin\theta(t) \neq 0$. This remains true (continuity is sufficient for this) even if $\sin\theta$ had vanished at some earlier time $t' < t$.

Acknowledgments. We wish to thank Ben Leimkuhler and Massimiliano Guzzo for useful discussions.

REFERENCES

[1] J. Barojas and D. Levesque, *Simulation of diatomic homonuclear liquids*, Phys. Rev. A, 7 (1973), pp. 1092–1105.
[2] G. Benettin and F. Fassò, *From Hamiltonian perturbation theory to symplectic integrators and back*, Appl. Num. Math., 29 (1999), pp. 73–87.
[3] G. Benettin and F. Fassò, *Fast rotations of the rigid body: A study by Hamiltonian perturbation theory. Part I*, Nonlinearity, 9 (1996), pp. 137–186.
[4] G. Benettin, F. Fassò and M. Guzzo, *Fast rotations of the rigid body: A study by Hamiltonian perturbation theory. Part II: Gyroscopic rotations*, Nonlinearity, 10 (1997), pp. 1695–1717.
[5] G. Benettin and A. Giorgilli, *On the Hamiltonian interpolation of near to the identity symplectic mappings, with application to symplectic integration algorithms.* J. Stat. Phys., 74 (1994), pp. 1117–1144.
[6] D. Evans, *On the representation of orientation space*, Mol. Phys., 34 (1977), pp. 317–325.

[7] D. Evans and S. Murad, *Singularity free algorithms for molecular dynamics simulation of rigid polyatoms*, Mol. Phys., 34 (1977), pp. 327–331.
[8] E. Hairer, *Backward analysis of numerical integrators and symplectic methods*, Ann. Num. Math., 1 (1994), pp. 107–132.
[9] E.J. Haug, *Computer Aided Kinematics and Dynamics of Mechanical Systems, Part I: Basic Methods*, Allyn & Bacon, Boston, 1989.
[10] D. Lewis and J.C. Simò, *Conserving algorithms for the dynamics of Hamiltonian systems on Lie groups.* J. Nonlinear Sci., 4 (1994), pp. 253–299.
[11] D. Lewis and J.C. Simó, *Conserving algorithms for the N dimensional rigid body.* Fields Inst. Comm., 10 (1996), pp. 121–139.
[12] A. Kol, B. Laird and B. Leimkuhler, *A symplectic method for rigid–body molecular simulation*, J. Chem. Phys., 107 (1997), pp. 2580–2588.
[13] B. Leimkuhler and S. Reich, *Symplectic Integration of Constrained Hamiltonian Systems*, Math. Comp., 63 (1994), pp. 589–605.
[14] B. Leimkuhler and R. Skeel, *Symplectic numerical integrators in constrained Hamiltonian systems*, J. Comp. Phys., 112 (1994), pp. 117–125.
[15] R.I. McLachlan, *Explicit Lie-Poisson integration and the Euler equations*, Phys. Rev. Lett., 71 (1993), pp. 3043–3046.
[16] S. Reich, *Momentum conserving symplectic integrators*, Physica D, 76 (1994), pp. 375–383.
[17] J. Touma and J. Wisdom, *Lie–Poisson integrators for rigid body dynamics in the solar system*, Astr. J., 107 (1994), pp. 1189–1202.
[18] H. Yoshida, *Construction of higher order symplectic integrators*, Phys. Lett. A, 150 (1990), pp. 262–268.
[19] H. Yoshida, *Recent progress in the theory and application of symplectic integrators*, Cel. Mech. and Dyn. Astr., 56 (1993), pp. 27–43.